NEW MATERIAL SYSTEMS FOR 3D CERAMIC PRINTING

Grant Marchelli, Mark Ganter, and Duane Storti
Department of Mechanical Engineering, University of Washington, Seattle, WA 98195

Reviewed, accepted September 15, 2009

Abstract

We present new material/binder systems for use in 3D printing hardware for the creation of mid-fire to high-fire ceramics. 3D printing is one of a variety of techniques in which objects are produced by printing binder onto a layer of powder. A brief overview of our process is presented and demonstration works are shown. Several available dry clay bodies were adapted for use in an existing, commercial 3D printer. Details of powder formulation are presented. Experimental results are presented for strain, flexural stress, and porosity for the various clay bodies as a function of firing temperature.

Keywords: 3D printing, new material/binder systems, mid-fire to high-fire ceramics

1. 3DP Introduction

3DP is a type of solid-freeform fabrication (SFF) that converts a digital CAD model to a tangible object by taking the model, slicing it into a predetermined number of layers (depending on the slicing parameters), and finally printing the model [7,12]. The object is built in a layer-by-layer fashion, using an inkjet printer that deposits droplets of binder activator the shape of a particular cross-section of the part to be produced, onto a bed of powder. Then, a roller or scraper adds a layer of powder atop the previously bound layer, and the process repeats until the part is complete [7,12]. 3DP has been in practice for a number of years and new applications are continually being discovered.

Numerous powder and binder combinations have been formulated and utilized in 3DP processes, and typical materials used include powdered metals, plasters, and ceramics, with binders generally containing some type of adhesive [7,12]. The material systems that we are presenting in this paper are new and unorthodox methods for producing three-dimensionally printed parts wherein the adhesive substance no longer resides in the liquid binder, but in the powder itself [8,11]. We have a desire to produce new powder/binder compositions in hopes of democratizing the 3DP niche by creating readily available materials, thereby increasing the breadth of applications lying outside of industry and academia [8]. More information regarding the testing and formulation of new material/binder combinations for use in 3DP can be found in past research and literature presented by Ganter, et al [11].

Ganter and collaborators developed the necessary powder/binder formulations to produce 3DP stoneware, terra cotta, and low-fire dry clay bodies, which can be purchased for reasonable prices [8]. The powder consists of dry clay bodies (i.e., stoneware slip), maltodextrin (a fiber supplement found at your local grocery store), and powdered sugar. The binder is comprised of distilled water, food-coloring (for troubleshooting purposes), and alcohol (found at your local liquor store) which acts as a surfactant to attain the proper binder viscosity and surface tension. As opposed to using an adhesive in the liquid binder, we decided that the best choice for this process was to use binder, namely maltodextrin and powdered sugar, in the powder itself. Using the powder as the binder as opposed to "jetting" the binder out of the print head is advantageous with respect to conventional 3DP (printing binder containing adhesives) for two main reasons: it

simplifies the problem domain and increases reliability. By printing a solvent that is inexpensive and easy to attain, we are able to increase the life of the print head, due to the lower viscosity and surface tension. Printing adhesives is very taxing on 3D print heads, but we have been successful in the general approach of printing a solvent as the liquid (binder activator). In particular, this tends to simplify the overall task of material system development to creation of the powder system. We are able greatly reduce the costs associated with the regular maintenance and upkeep of 3DP's. Increasing the life of the print head, in addition to decreasing the costs of materials (both binder and powder), equates to affordable 3DP.

By weight, the powder is made up of approximately 66.6% dry clay body, 16.7% maltodextrin, and 16.7% powdered sugar [8]. This formula is the result of prior testing, and was chosen because of the *green* strength of the parts. For the duration of this paper, green parts will refer to objects that have been 3D printed, but not fired, and brown parts will refer to objects that have been both printed and fired. Using organic substances in the material system can present difficulties later in the process, such as increased strain (shrinkage) due to the organics being burned out during sintering.

A number of very different operations go into successfully producing a 3D printed and sintered part. Our goal was to create new material systems for use in 3DP technologies that would incorporate dry clay bodies fired at mid to high temperatures (1149-1316˚C). The effects of sintering have been partially explored using our 3DP ceramic material systems, namely, porcelain and stoneware. A maximum sintering temperature of 1316˚C was used based on the properties of porcelain, which is a high temperature, non-engineering ceramic that is rated as a cone 11 (1316˚C) dry clay body. Stoneware, a mid temperature, non-engineering ceramic is rated as a cone 7 (1240˚C) dry clay body. In addition, the Orton AutoFire kiln used for firing the specimens was rated at a maximum temperature of 1316˚C, and so data beyond this temperature were not explored. In order to achieve temperatures greater than 1316˚C, a more expensive kiln would be necessary. For this initial, experimental investigation of the properties of the sintered 3DP ceramics presented in this paper, we employ a simple fast firing sintering schedule (see *Figure 1*) and focus on the effects of a single variable, peak sintering temperature.

Once a new material/binder system had been realized for use in 3DP, it was desirable to understand the characteristics of the parts produced by conducting a series of engineering tests. The analysis of two dry clay bodies, porcelain and stoneware, produced by 3DP has been performed to reveal strain, flexural stress, and porosity as functions of peak sintering temperature. The green test specimens were printed, put through a drying cycle, measured, and then kiln fired. Upon completion of firing, the specimens were cooled and experiments for the aforementioned properties were performed.

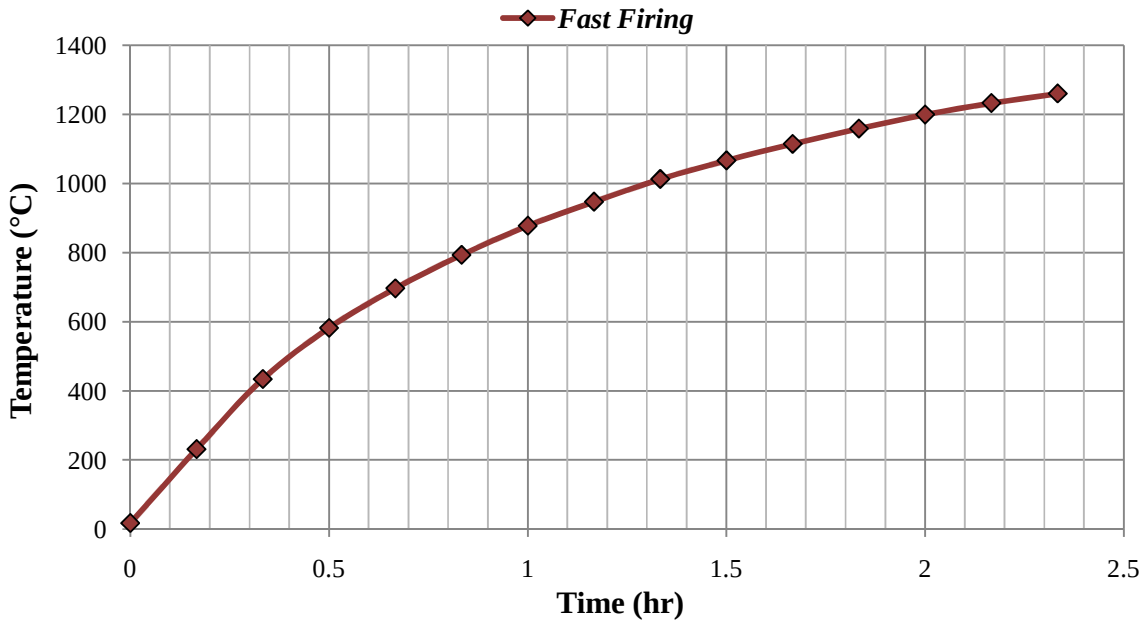

Figure 1: *Fast firing heating schedule with a peak temperature of 1260°C. The fast firing schedule was plotted using 10-minute intervals, while the kiln was heating at its maximum rate. The curve is logarithmic in nature and experiences asymptotic behavior as the kiln temperature approaches the desired input value.*

3. Strain Experimentation

To determine the amount of linear strain experienced in the two types of ceramic materials, numerous "test bars" were printed based on a 3D CAD model of a 10x10x100 mm bar. The 100 mm length was built parallel to the fast axis (conventionally, the y-direction) defined by the movement of the inkjet print head on the gantry style 3D printer. (Conversely, the slow axis conventionally, the x-direction) is defined by the movement of the entire printer assembly). This orientation was chosen to increase the green strength of the samples [1,2,7,8,11].

3.1 Experimental Setup

A total of six test bars per firing temperature were printed per ASTM standards on testing *whiteware* (i.e., porcelain). ASTM suggests that a minimum of five specimens should be tested for each data point, but variability in printing behavior led to decision of six specimens per point. Cross-sectional area measurements of the green bars were taken at three different points along the bars using digital calipers, and the heights and widths of the bars were recorded. After measuring all of the bars, the average cross-sectional area was calculated, and the formulation of a *representative length* proceeded. Representative length, L_R, for a bar of height h and width w is given by:

$$L_R = (hw)^{1/2} \tag{1}$$

The representative length was used to produce more accurate linear strain when compared to conventional linear strain, which uses L_o, the original length, and ΔL, the change in length with respect to time or temperature [1,2,4,5,10]. Strain, ε, is a dimensionless material

property that is defined by the change in length per unit length, and can also be referred to as shrinkage when dealing with percentages [4]. For the remainder of this paper, we will refer to linear strain resulting from firing as final sintering strain. Since we have adapted new material systems to 3DP, and due to the unavailability of prior research, we decided to take the representative approach for acquiring final sintering strain ($\Delta L_R/L_R$). Final sintering strain curves for the porcelain and stoneware clay bodies are presented in *Figure 2*.

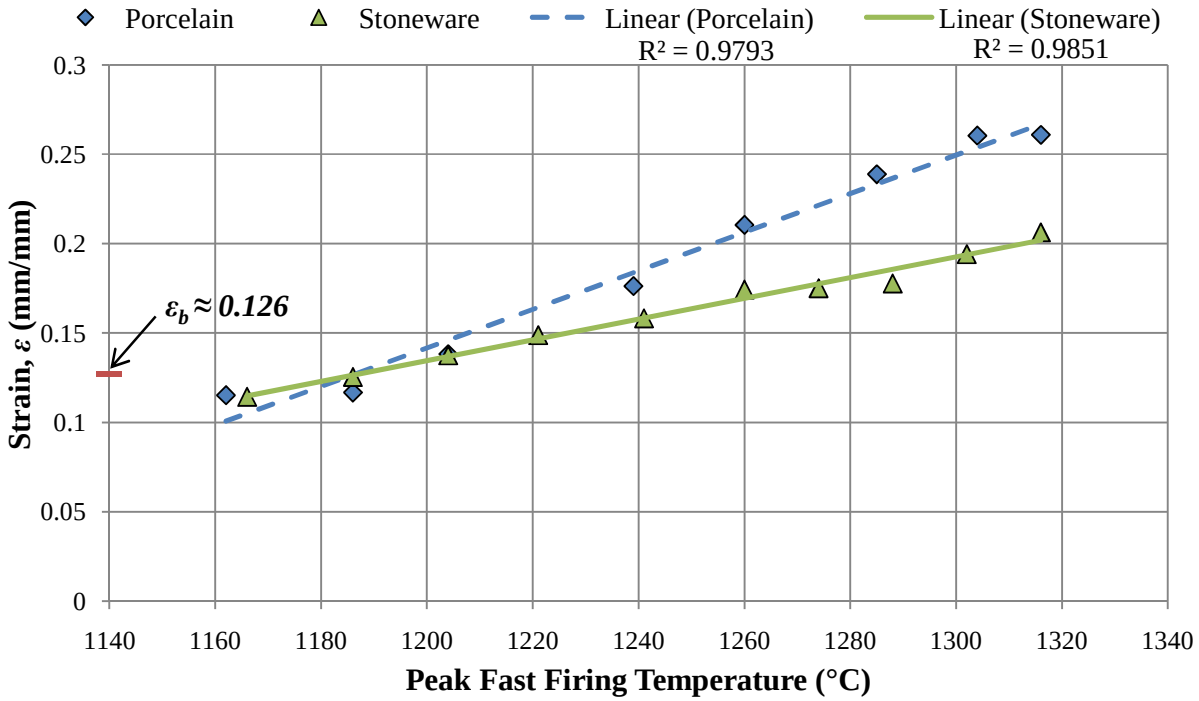

Figure 2: *Final sintering strain as a function of peak firing temperature. The plot indicates that both porcelain and stoneware experience a linear sintering strain-temperature relation, with porcelain having a greater sensitivity to higher sintering temperatures resulting in a steeper curve. The point,* ε_b*, refers to the quantity of strain that occurs due to the organic binder burning out. Strain beyond this threshold is attributed to the sintering mechanism.*

3.2 Discussion of Strain Experiment Results

As can be seen in *Figure 2*, a linear model describes the dependence of strain on peak sintering temperature with a high coefficient of determination, R^2, exceeding 98% for both the porcelain and the stoneware [18]. Equations for the linear models are $\varepsilon_p = 0.0011T\text{-}1.1526$ and $\varepsilon_s = 0.0006T\text{-}0.5632$ for the porcelain and stoneware, respectively. The maximum sintering strain experienced in the porcelain specimens was 0.261 mm/mm, as compared to that of the stoneware at 0.206 mm/mm. The results indicate that while porcelain is qualified as a high-fire clay body, and stoneware as a mid-fire clay body, the rate at which porcelain experiences strain is slightly higher than stoneware (refer to *Figure 2*).

At the two lowest fast firing temperatures, 1162°C and 1186°C, final strain is largely attributed to the organic binder burning out. Since the parts are comprised of 1/3 organic material by volume (maltodextrin and sugar), and all of that volume theoretically burns off during firing,

the parts should shrink 12.6%. This value does not include shrink caused by initial stage sintering, which is defined by the presence of neck growth in adjacent (powder) particles, and marks an object's transition from green to brown [1,3,5,10]. Typically, initial stage sintering only produces shrinkage values of 0-3%, therefore shrinkages below 15.6% are caused by initial stage sintering combined with organic binder burnout [1,3,10]. Shrinkage above approximately 15.6% is a result of intermediate/final stage sintering, in addition to binder burnout. The bars that were sintered at lower temperatures were extremely weak, and particles were easily shed from the surface during handling. As the peak temperature increased, the test bars became more robust, and sloughing (loss of material via handling or small frictional forces) was nonexistent. This transition occurred at approximately 1288°C and 1250°C for the porcelain and stoneware, respectively. When the bars were dropped or tapped, the characteristic "ring" of a ceramic was heard. As the peak temperature increased, the bars rang at higher pitches.

4. Flexural Stress Experimentation

4.1 Experimental Setup

The test specimens used for the flexural stress experiment were taken after completion of the strain testing, therefore, the bars had green dimensions of 10x10x100 mm and brown dimensions as measured during the strain curve formulations. In this experiment, the test samples were placed on an Instron 5585H stress testing machine, and were subjected to a load until failure (*Figure 3*). In a three point bend test setup, the load cell on the Instron was calibrated to move towards the specimen at a rate of 1 mm per minute, and the specimens were simply supported with a distance between support center points equal to 50 mm. The procedure was repeated with every test sample and the following data was gathered; maximum flexural load, flexural stress at maximum flexural load, and flexural extension at maximum load. Maximum flexural stress is defined as the maximum fiber stress, or the maximum stress at the outer most fiber of the specimen at peak loading [4,16]. Graphs were created using the flexural stress at maximum load versus peak fast firing temperature, and corresponding equations can be found in the literature [4,16].

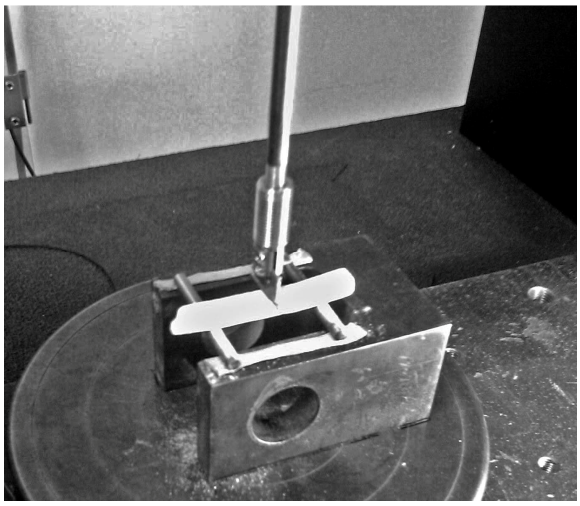

Figure 3: *Experimental set up for the three point bend test using the Instron.*

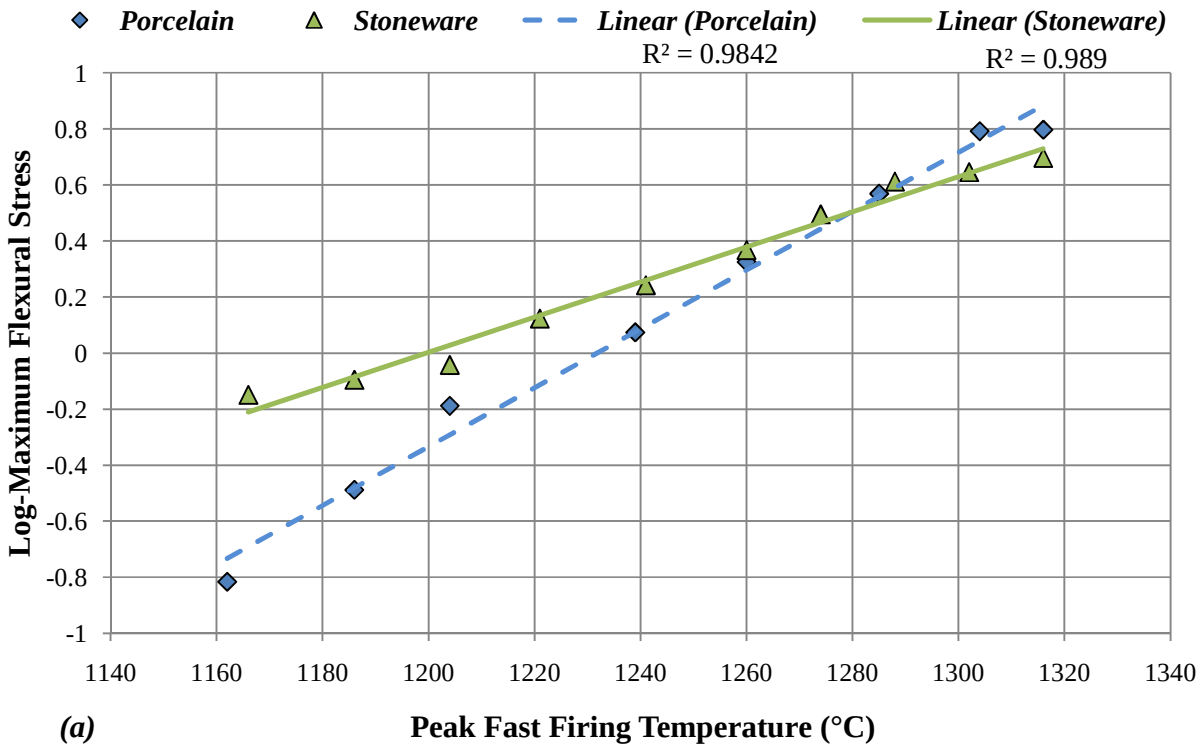

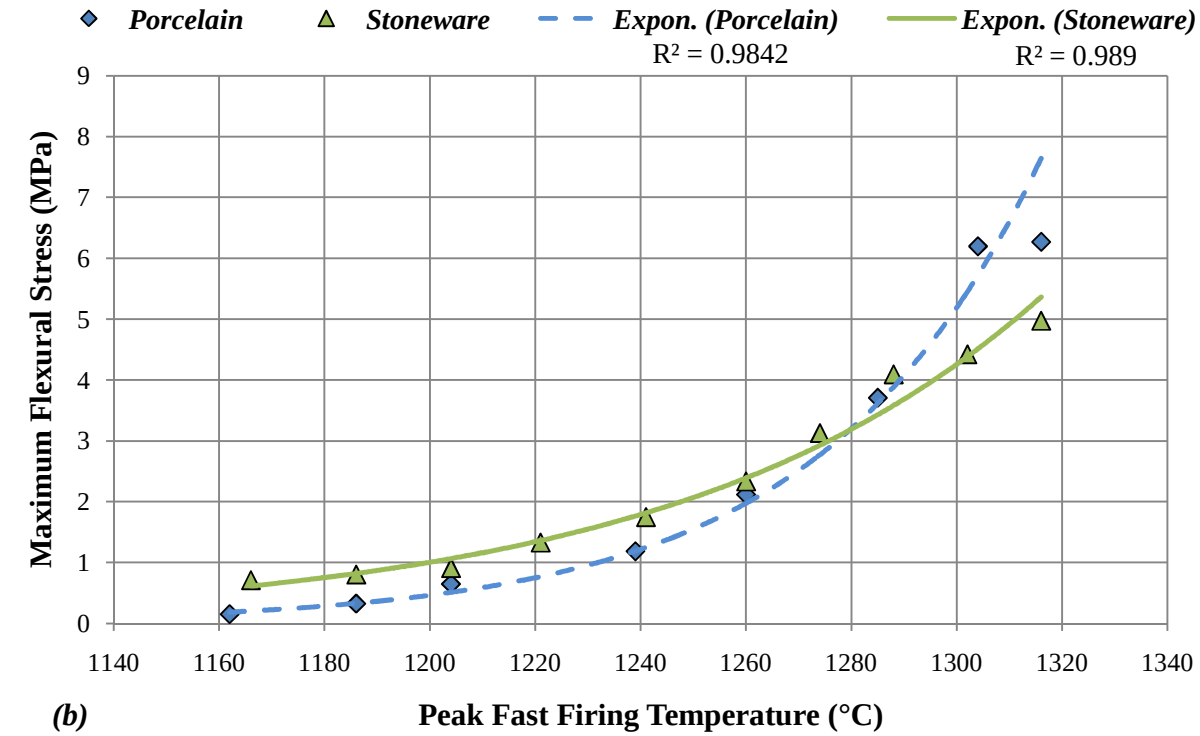

Figure 4: *Linear models (a) of log of maximum flexural stress versus peak temperature with high coefficients of determination (R^2 > 0.98) establish exponential relations shown in (b).*

4.2 Discussion of Flexural Stress Experiment Results

Using a linear model, R^2 values of 0.93 and 0.87 were found for the porcelain and stoneware, respectively. The results indicate that a linear model is a non-optimal approximation and an alternative method should be employed [18]. In *Figure 4a*, it can be seen that by plotting the log of the maximum flexural stress versus peak fast firing temperature, and applying a linear fit, much higher R^2 values were attained. The R^2 values for the log plot were 0.98 and 0.99, for the porcelain and stoneware, respectively. By verifying that the linear model for the log plot was a good approximation, we were able to justify the application of an exponential model to the data (*Figure 4b*). The results show high coefficients of determination, exceeding 98%, for the exponential growth experienced by both the porcelain and stoneware, indicating accurate models were realized.

We were only able to find limited data regarding the maximum flexural stress of porcelain and stoneware clay bodies. Prior investigation into tensile and compressive strength was performed by Moore [15], and the ultimate stress, σ_u, was revealed for porcelain and stoneware. Accepted published values for the ultimate tensile stress are $\sigma_u \geq 20.7$ MPa (≥ 3000 psi) and 7.84-15.2 MPa (1100-2200 psi) for porcelain and stoneware, respectively [15]. Since ceramics are considered brittle materials, ultimate tensile stress is comparable to maximum flexural stress, because brittle materials do not experience necking, and therefore, do not experience a significant change in cross-sectional area during loading. The ultimate stress for 3DP porcelain and stoneware was achieved at 1316°C, and values for the porcelain and stoneware were 6.27 MPa and 4.97 MPa, respectively. The data signifies that 3DP porcelain and stoneware, which are porous in nature (discussed in the following section), can attain ultimate stress values of approximately 1/3 of the accepted published values. While the 1/3 number is consistent between materials, further testing will be required to determine if our 3DP materials and process match existing models for strength versus porosity [17].

5. Porosity and Bulk Density Experimentation

All powder material systems which are subjected to sintering techniques undergo a process known as densification [1,3,5,10]. Densification within the specimen occurs due to a number of processes including neck growth, grain growth, and pore shrinkage [1,3,5,10]. During the early stages of sintering (adhesion and initial), German [10] reveals that necking occurs within the loose powder particles, which signifies that the specimen has begun densification. During the intermediate stage of sintering, pores within the body begin to elongate, and this elongation has a significant effect on the densification rate of the porous powder body [10]. Final stage sintering has minimal effects on the density of the body, and pores ultimately are engulfed by grain growth or remain as closed pores within the body [1,3,5,10]. For this experiment, test subjects with cubical geometries were printed using the stoneware material system, and fast fired at various temperatures (1204-1316°C). The porosity of the stoneware specimens was then measured according to ASTM standard C 373-88.

5.1 Experimental Setup

Upon completion of the aforementioned fast firing sintering methods, the specimens were dried to a constant mass. The dry mass, *D*, was recorded, followed by placement of the specimens into a pan of distilled water. The samples were then boiled for a total of 5 hours (in the distilled water), and were allowed to soak in the water for an additional 24 hours, to allow for

complete impregnation of the distilled water into the specimens. Once the specimens had reached maximum saturation, they were weighed while being suspended in a bath of distilled water. Let the mass of the cubes (specimens) while suspended in water be denoted as *S*. Next, it was necessary to determine the mass of the saturated specimen, *M*, while being weighed in air. After *D*, *S*, and *M* were recorded, the calculations for apparent porosity, *P*, and bulk density, *B*, could be performed using the following equations:

$$V = (M - S)/\rho_w \tag{2}$$

where *V* is the exterior volume of the specimen, and *M* and *S* are previously defined as saturated mass and suspended mass, respectively. The density of water, ρ_w, was measured to be 0.998 g/cm^3 at 20.5°C. The apparent porosity, *P*, which is the relationship of the volume of open pores to the exterior volume of the sample, could be determined using:

$$P = [(M - D)/V\,]\text{x}100 \tag{3}$$

where *M*, *D*, and *V* are saturated mass, dry mass, and exterior volume, respectively [9]. Using the information from Equation (3), the relative density, ρ, was determined as follows:

$$\rho = 1 - P \tag{4}$$

Once *V*, the exterior volume was known, calculations of the bulk density, *B*, in grams per cubic centimeter (g/cm^3) were performed using:

$$B = D/V \tag{5}$$

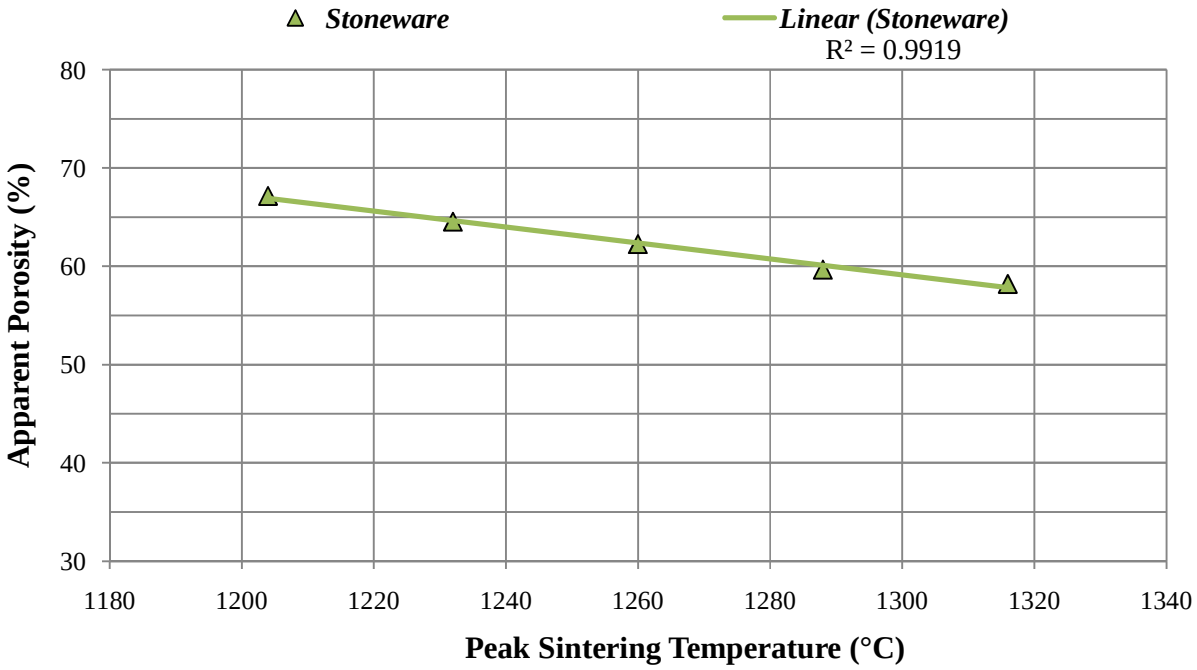

Figure 5: *Apparent porosity as a function of peak temperature.*

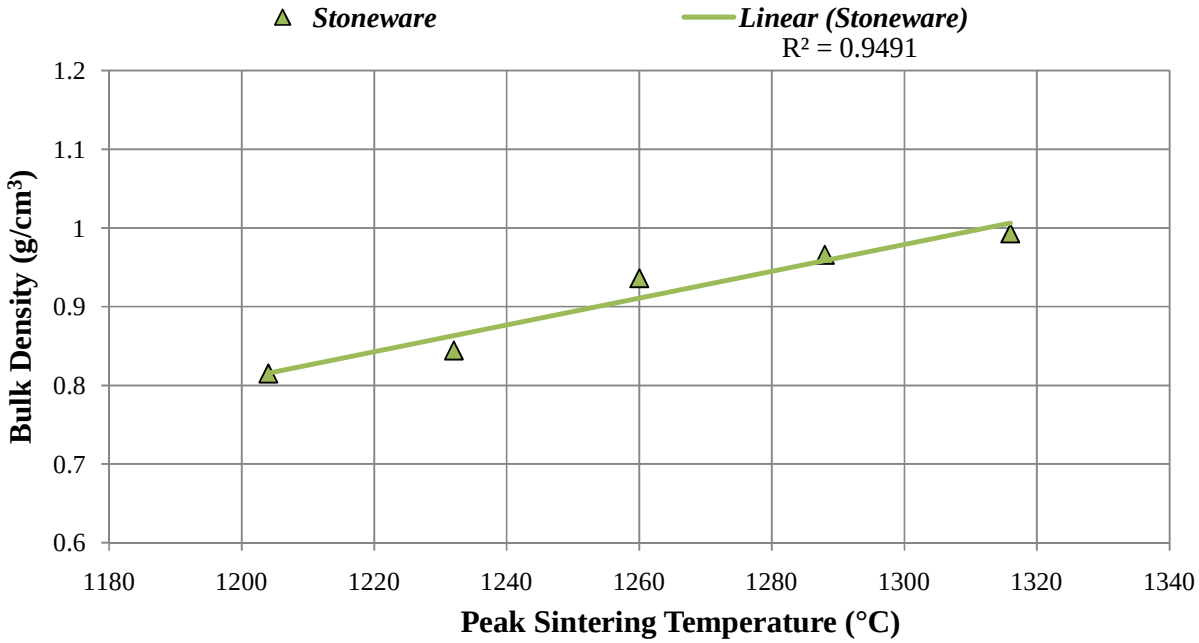

Figure 6: *Bulk density as a function of peak temperature.*

5.2 Discussion of Porosity and Bulk Density Results

Using a linear model for the apparent porosity versus peak temperature, an R^2 value of 0.99 was achieved, indicating an accurate fit. The equation for the apparent porosity is $P_a = -0.046T+168.84$. Brown parts manufactured in a 3DP powder environment are only capable of reaching relative densities of 40-60%, that is, without any external forces applied such as mechanical compaction or by using a pressurized atmosphere [13,14]. Referring to *Figure 5*, it can be seen that a maximum porosity of 67.2% was reached at a sintering temperature of 1204°C, therefore indicating a minimum relative density of 32.8% in the stoneware material system. Also, a minimum porosity of 58.2% at 1204°C was achieved, resulting in a maximum relative density of 41.8%. Previous work by Sachs [13] reveals a packing density of approximately 50%, and the relative densities of the 3DP stoneware system are approximately 20% lower than the expected 40-60%. This is directly related to the aforementioned ceramic process in which our system is comprised of 33% organic materials. During the firing, organics burn out of the green part at temperatures in the 232-482°C range, therefore our parts lose approximately 1/3 of their green volume [1]. Taking this into account, it was expected that our material systems attain a relative density of between 20-40%. In terms of bulk density, *B*, the stoneware system started at a minimum value of 81.5% of the bulk density of water, 0.815 g/cm^3, at 1204°C. At the 1316°C (refer to *Figure 6*), the bulk density of the stoneware system was 0.993 g/cm^3, nearly equivalent to the density of water at the measured temperature of 20.5°C (0.998 g/cm^3).

6. Conclusions

This paper presented experimental measurements of engineering properties for 3DP porcelain and stoneware. Experimental data was presented for strain, flexural stress, and porosity as a function of peak fast firing. Data reveals that the strain-temperature relation for both

porcelain and stoneware follows a linear curve. Porcelain is subject to higher values of strain than stoneware, but it is stronger, which is expected of high-fire (porcelain) versus mid-fire (stoneware) ceramics. Flexural stress values for the stoneware approach 1/3 of the quantities found using conventional manufacturing techniques (i.e., fully dense), foreshadowing possible future applications. Density testing of the stoneware is consistent with prior research indicating that a maximum of 40-60% apparent density can be attained in 3DP processes. While other SFF processes can achieve 40-60% apparent density, using our material system consisting of 33% organic materials, an apparent density of 20-40% is attained.

Using the fast firing heating scheduled, kiln runs last roughly 2 hours, and cost between $0.20 and $0.40 per run. This inexpensive heating schedule, combined with reasonably priced materials, and the increased lifespan of the 3DP system components allows for high volume, and various material testing that could not be done otherwise. By sharing this information, we hope to democratize the 3DP process, and make available this intriguing technology to a larger audience via introduction of new materials.

7. Acknowledgements

We would like to thank our staff engineer, Bill Kuykendall, for his assistance with setting up the three point bend tests using the Instron, and gathering instrumentation for porosity tests.

8. References

1. S. Johnston (2005), Initial Stage Sintering Model of 316L Stainless Steel with Application to Three Dimensionally Printed (3DP™) Components, (pp. 10-11, 25-30), Doctoral Dissertation, University of Washington.
2. A. Gebhardt (2003), *Rapid Prototyping*, Munich: Hanser Publishers.
3. M.N. Rahaman (2008), *Sintering of Ceramics*, (pp. 1-6, 208-214, 305-335), Boca Raton: CRC Press.
4. M. R. Lindeburg (2004), *FE Review Manual*, Belmont: Professional Publications, Inc., (pp. 20.1-20.4).
5. G.C. Kuczynski (1979). Sintering Processes. *Proceedings of the fifth International Conference on Sintering and Related Phenomena, June 18-20*. New York: Plenum Press.
6. S. F. Pond (2000), *Inkjet Technology and Product Development Strategies*, Carlsbad: Torrey Pines Research.
7. E. Sachs, P. Williams, D. Brancazio, M. Cima, & K. Kremmin (1990). Three Dimensional Printing: Rapid Tooling and Prototypes Directly from a CAD Model. In B. Frost (Ed.) & M. Jamshida (Ed.), *Advances in Materials and Automation*. *Proceedings of Manufacturing International '90*, (pp. 131-136). New York: United Engineering Center.
8. M. Ganter, D. Storti, & B. Utela (2009), The Printed Pot: with recipes for Printing Slips. *Ceramics Monthly, February 2009*, (pp. 36-39).
9. ASTM (2006), Designation C 373-88: *Standard Test Method for Water Absorption, Bulk Density, Apparent Porosity, and Apparent Specific Gravity of Fired Whiteware Products*, West Conshohocken: ASTM International.
10. R.M. German (1996), *Sintering Theory and Practice*, (pp. 8-12, 98-102, 335-338), New York: John Wiley & Sons, Inc.,
11. B. Utela, D. Storti, R. Anderson, & M. Ganter (2008), A review of process development steps for new material systems in three dimensional printing (3DP). *Journal of Manufacturing Processes, Volume 10, Issue 2*, (pp. 96-104).
12. E. Sachs et al. (1993). Three-dimensional printing techniques. *U.S. Patent No. 5,204,055*. Washington, D.C.: U.S. Patent and Trademark Office.
13. E. Sachs et al. (2003). Jetting layers of powder and the formation of fine powder beds hereby. *U.S. Patent No. 6,596,224*. Washington D.C.: U.S. Patent and Trademark Office.
14. S. Baskaran et al. (1996). Method of freeform fabrication by selective gelation powder suspensions. *U.S. Patent No. 5,697,043*. Washington D.C.: U.S. Patent and Trademark Office.
15. H.F. Moore (1953). *Text-book of the Materials of Engineering*, (pp. 193), New York: McGraw-Hill.
16. Instron online. www.instron.com/.
17. W. Fehghui, Z. Xiulin, & L. Mingxu (1995). On the Strength of Ceramics with Cavities. *International Journal of Fracture, 70*, (R19-R22).
18. D.C. Montgomery & G.C. Runger (2007). *Applied Statistics and Probability for Engineers*, (pp. 418), Hoboken: John Wiley & Sons, Inc.